# Capture of Carbon Dioxide from Air and Flue Gas in the Alkylamine-Appended Metal-Organic Framework mmen-Mg-2(dobpdc)

**ARTICLE** *in* JOURNAL OF THE AMERICAN CHEMICAL SOCIETY · APRIL 2012

Impact Factor: 12.11 · DOI: 10.1021/ja300034j · Source: PubMed



**6 AUTHORS**, INCLUDING:

Woo Ram Lee
Korea University
**29** PUBLICATIONS **591** CITATIONS
SEE PROFILE

Brian M Wiers
University of California, Berkeley
**9** PUBLICATIONS **522** CITATIONS
SEE PROFILE

JACS
JOURNAL OF THE AMERICAN CHEMICAL SOCIETY
Article
pubs.acs.org/JACS

# Capture of Carbon Dioxide from Air and Flue Gas in the Alkylamine-Appended Metal–Organic Framework mmen-$Mg_2$(dobpdc)

Thomas M. McDonald,[†] Woo Ram Lee,[§] Jarad A. Mason,[†] Brian M. Wiers,[†] Chang Seop Hong,*[,§] and Jeffrey R. Long*[,†]

[†]Department of Chemistry, University of California, Berkeley, California 94720, United States
[§]Department of Chemistry, Research Institute for Natural Sciences, Korea University, Seoul 136-713, Republic of Korea

Supporting Information

**ABSTRACT:** Two new metal–organic frameworks, $M_2$(dobpdc) (M = Zn (**1**), Mg (**2**); dobpdc$^{4-}$ = 4,4′-dioxido-3,3′-biphenyldicarboxylate), adopting an expanded MOF-74 structure type, were synthesized via solvothermal and microwave methods. Coordinatively unsaturated $Mg^{2+}$ cations lining the 18.4-Å-diameter channels of **2** were functionalized with *N*,*N*′-dimethylethylenediamine (mmen) to afford $Mg_2$(dobpdc)-$(mmen)_{1.6}(H_2O)_{0.4}$ (mmen-$Mg_2$(dobpdc)). This compound displays an exceptional capacity for $CO_2$ adsorption at low pressures, taking up 2.0 mmol/g (8.1 wt %) at 0.39 mbar and 25 °C, conditions relevant to removal of $CO_2$ from air, and 3.14 mmol/g (12.1 wt %) at 0.15 bar and 40 °C, conditions relevant to $CO_2$ capture from flue gas. Dynamic gas adsorption/desorption cycling experiments demonstrate that mmen-$Mg_2$(dobpdc) can be regenerated upon repeated exposures to simulated air and flue gas mixtures, with cycling capacities of 1.05 mmol/g (4.4 wt %) after 1 h of exposure to flowing 390 ppm $CO_2$ in simulated air at 25 °C and 2.52 mmol/g (9.9 wt %) after 15 min of exposure to flowing 15% $CO_2$ in $N_2$ at 40 °C. The purity of the $CO_2$ removed from dry air and flue gas in these processes was estimated to be 96% and 98%, respectively. As a flue gas adsorbent, the regeneration energy was estimated through differential scanning calorimetry experiments to be 2.34 MJ/kg $CO_2$ adsorbed. Overall, the performance characteristics of mmen-$Mg_2$(dobpdc) indicate it to be an exceptional new adsorbent for $CO_2$ capture, comparing favorably with both amine-grafted silicas and aqueous amine solutions.

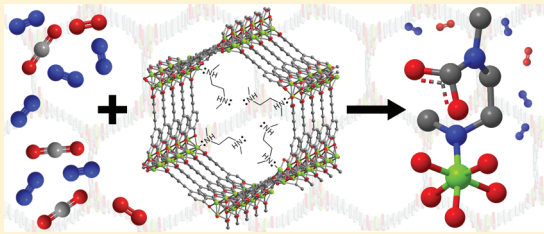

## 1. INTRODUCTION

The concentration of $CO_2$ in the Earth's atmosphere is presently 390 ppm,[1] an increase of approximately 110 ppm since the start of the Industrial Revolution.[2] The combustion of fossil fuels is largely responsible for this increase,[3] yet fossil fuels will continue to be heavily utilized for energy production during the 21st century. Currently, there is significant interest in the development and implementation of technologies that slow $CO_2$ emissions and thus forestall the most severe consequences of global warming. For limiting future $CO_2$ emissions from large, stationary sources like coal-fired power plants, carbon capture and sequestration (CCS) has been proposed.[4] The CCS process involves the selective removal of $CO_2$ from gas mixtures, the compression of pure $CO_2$ to a supercritical fluid, transportation to an injection site, and finally permanent subterranean or submarine storage.[5] For the retrofit of existing power plants, post-combustion $CO_2$ capture is a likely configuration. In this design, fuel is burned in air and $CO_2$ is removed from the effluent. For coal-fired power plants, the largest flue gas components by volume are $N_2$ (70–75%), $CO_2$ (15–16%), $H_2O$ (5–7%), and $O_2$ (3–4%), with total pressures near 1 bar and temperatures between 40 and 60 °C.[6]

Aqueous amine solutions are currently the most viable absorbents for carbon capture under the aforementioned conditions, and they are presently used for the removal of $CO_2$ from industrial commodities like natural gas.[7] While a variety of advanced amines are available, 30% monoethanolamine (MEA) in water is the benchmark solvent against which competing technologies are generally compared. The low solvent cost and proven effectiveness make MEA an attractive absorbent for many applications. However, if MEA were to be utilized for CCS, electricity prices are projected to increase by 86%.[8] The U.S. Department of Energy has targeted a maximum 35% increase for the cost of electricity produced from a coal power plant that captures 90% of the $CO_2$ it generates. The diversion of steam from the electricity generation cycle to the solvent regeneration cycle sharply reduces the net electricity output of the plant, drastically increasing electricity costs. Previous work has demonstrated that plant efficiency is highly dependent on the solvent regeneration energy.[9]

Presently, there is significant interest in the development of solid adsorbents that selectively adsorb $CO_2$ at partial pressures applicable to CCS.[10] Solid adsorbents are promising candidates because the significantly smaller heat capacities of solids may reduce the sensible heat required for regeneration. In addition, solvent loss and corrosion issues resulting from the use of aqueous amines would be minimized if solids adsorbents were instead utilized.[9]

**Received:** January 2, 2012
**Published:** April 4, 2012

   dx.doi.org/10.1021/ja300034j | *J. Am. Chem. Soc.* 2012, 134, 7056–7065

While CCS is perhaps unlikely to be widely implemented within the next decade,[5] a number of current industrial processes utilize liquid or solid adsorbents to remove $CO_2$ from gas mixtures. These processes could benefit greatly from the next generation of adsorbents that are currently being proposed for CCS applications. Currently, aqueous amines are used industrially to separate $CO_2$ from gas mixtures with high $CO_2$ partial pressures like natural gas, while solid adsorbents are used to remove $CO_2$ from mixtures with very low $CO_2$ partial pressures.

Among the most challenging $CO_2$ separations is the removal of $CO_2$ directly from air. Prior to the cryogenic distillation of air for $N_2$, $O_2$, and Ar production, $CO_2$ is removed from the air to minimize solid $CO_2$ formation on heat exchangers.[11] To maximize the capacity of zeolite 13X for $CO_2$ adsorption, the air stream is dried over alumina, cooled to 5 °C, and pressurized to 5−7 bar. The effective capacity of zeolite 13X, the most widely used adsorbent for this process, under these conditions is ca. 0.35 mmol/g, which corresponds to a crystallographic volumetric capacity of approximately 0.5 mmol/cm$^3$.[11c,12] In this "pre-purification" step, the $CO_2$ concentration in the air is reduced to less than 1 ppm. New higher-capacity adsorbents could potentially eliminate the costs associated with pre-cooling feed air and reduce the adsorbent regeneration energy.

Carbon dioxide scrubbers are critical life support systems in confined spaces with limited air exchange, such as spacecraft, submarines, and breathing suits.[13] Because of the very low capacity of solid adsorbents for 390 ppm $CO_2$ in unpressurized gas streams, weight and volume limitations prevent the implementation of systems capable of maintaining $CO_2$ concentrations at atmospheric levels. Thus, the average $CO_2$ concentration aboard the International Space Station ranges from 3000 to 7000 ppm,[14] which approaches the currently established safe limit for chronic $CO_2$ exposure.[14,15] Improved adsorbents could potentially reduce $CO_2$ concentrations within confined spaces to significantly lower and potentially safer levels, while simultaneously reducing the adsorbent mass and volume.

In addition to current processes that remove $CO_2$ from air, proposed technologies may benefit greatly from improved air capture adsorbents. For example, alkaline fuel cells (AFCs)[16] and iron-air batteries[17] require $CO_2$-free $O_2$ sources to avoid electrolyte side reactions. It has been previously suggested that improved $CO_2$ adsorbents could solve many issues associated with the operation of AFCs because air purification imposes considerable engineering and financial burdens on the system.[18]

Lastly, directly adsorbing $CO_2$ from the atmosphere combined with geologic sequestration has been proposed as a potential solution for offsetting $CO_2$ emissions from mobile or diffuse generators.[19] Direct air capture, if widely implemented, could also theoretically reduce atmospheric $CO_2$ concentrations by capturing historic emissions rather than simply abating future emissions. Significant obstacles remain for direct air capture including its substantially higher cost compared to traditional CCS.[20] Yet many estimates rely on the use of traditional inorganic bases, which require the construction of very large physical structures to ensure sufficient surface area for air to contact the adsorbent.[21] Porous solid adsorbents with high surface areas could potentially drastically reduce the large capital costs associated with air capture.

Recently, amine-functionalized porous solids have been proposed as superior adsorbents for air capture compared to inorganic bases and zeolites. For example, amine-modified porous polymers have been tested for use aboard spacecraft.[22] Silica,[17,23] alumina,[24] and carbon[25] adsorbents functionalized with amines have also been analyzed for their efficacy as air capture adsorbents, as have ammonium ion-exchange membranes.[26] The primary advantage of amine-functionalized adsorbents is their high capacity for 390 ppm $CO_2$, in some cases in excess of 2 mmol/g. However, existing materials of this type frequently require hours to reach saturation because of slow adsorption kinetics.

Metal−organic frameworks are a class of porous, crystalline adsorbents that have recently attracted much attention for use in gas separations.[10,27] The high tunability of their design may enable greater functionality with reduced adsorbent mass and volume compared to traditional solid adsorbents. Among the most interesting features of some metal−organic frameworks is the presence of coordinatively unsaturated metal centers (open metal sites) along the pore surfaces.[28,29] These five-coordinate metal cations, known to behave as Lewis acids that strongly polarize gas adsorbents, are further amenable to post-synthetic functionalization.[30]

In chemically robust metal−organic frameworks with well-separated open metal sites, one amine of a diamine molecule can bind to a metal cation as a Lewis base, while the second amine remains available as a chemically reactive adsorption site. The modification of open metal sites within the metal−organic framework Cu-BTTri with the secondary amine *N,N′*-dimethylethylenediamine (mmen) was recently reported.[31] Upon grafting mmen onto the exposed $Cu^{2+}$ sites of the framework, a 3.5 times enhancement in $CO_2$ capacity at 0.15 bar and 25 °C was realized. We believe that the incorporation of very basic alkylamines into framework pores will be a promising strategy for increasing the capacity of metal−organic frameworks for $CO_2$ uptake at low partial pressures.

The high concentration of open metal sites within the $M_2$(dobdc) (M = Mg, Mn, Fe, Co, Ni, Zn; dobdc$^{4-}$ = 2,5-dioxido-1,4-benzenedicarboxylate; M-MOF-74 or CPO-27-M) series of metal−organic frameworks makes them attractive candidates for diamine functionalization.[29] To date, however, we have been unable to synthesize promising amine functionalized derivatives of the $M_2$(dobdc) series. We hypothesized that the relatively narrow, one-dimensional channels (~11 Å diameter) may be hindering effective diffusion of the diamines into the framework. Thus, we sought to synthesize expanded analogues of the $M_2$(dobdc) structure via a ligand extension. Larger pores should enable more facile functionalization, enhance gas diffusion, and potentially unlock unrealized functionality within this interesting structural topology replete with open metal sites.

Herein, we report the first expanded analogues of the $M_2$(dobdc) structure type, featuring 18.4-Å-wide channels and exhibiting exceptional $CO_2$ adsorption properties upon functionalization with mmen.

## 2. EXPERIMENTAL SECTION

**General.** All reagents were obtained from commercial vendors at reagent grade purity or higher and used without further purification.

*4,4′-Dihydroxy-(1,1′-biphenyl)-3,3′-dicarboxylic Acid ($H_4$dobpdc).* The compounds 4,4′-dihydroxybiphenyl (1.16 g, 6.24 mmol), $KHCO_3$ (2.00 g, 20.0 mmol), dry ice (4 g), and 1,2,4-trichlorobenzene (3 mL) were added to a PTFE insert within a steel acid digestion bomb (23 mL) and heated at 255 °C for 17 h.[32] After cooling to room temperature, the mixture was collected via vacuum filtration and washed with diethyl ether. The solid was suspended in 300 mL of


dx.doi.org/10.1021/ja300034j | J. Am. Chem. Soc. 2012, 134, 7056−7065

distilled water and filtered again. To the filtrate, neat HCl was slowly added until a pH between 1 and 2 was reached. The resulting crude product was collected via filtration. Recrystallization using 50 mL of acetone and 50 mL of water per gram of crude material afforded 0.68 g (40%) of pure product as a white powder. Anal. Calcd for $C_{14}H_{10}O_6$: C, 61.32; H, 3.68. Found: C, 61.34; H, 3.60. IR (KBr) 1659 (vs), 1612 (s), 1481 (s), 1450 (vs), 1319 (s), 1290 (s), 1240 (s), 1099 (w), 1047 (w), 894 (w), 825 (m), 792 (m), 723 (w), 686 (m), 573 (w), 530 (w) $cm^{-1}$. $^1H$ NMR (300 MHz, dmso-$d_6$): $\delta$ = 10.75−11.95 (br, 2H), 7.93 (s, 2H), 7.74 (d, 2H, $J$ = 11.2 Hz), 7.00 (d, 2H, $J$ = 8.6 Hz).

*$Zn_2$(dobpdc)(DEF)$_2$·DEF·$H_2O$ (DEF-1).* To a 2-mL Pyrex tube, $H_4$dobpdc (4.0 mg, 0.015 mmol), $ZnBr_2·2H_2O$ (8.9 mg, 0.034 mmol), and 0.5 mL of mixed solvent (1:1 DEF:EtOH; DEF = *N*,*N*-diethylformamide) were added. The tube was sealed and placed in a pre-heated oven at 100 °C. After 72 h, needle-shaped, colorless crystals had formed. The crystals were isolated by filtration and washed with hot DEF to afford 3.7 mg (35%) of product. Anal. Calcd for $C_{29}H_{41}N_3O_{10}Zn_2$: C, 47.84; H, 5.64; N, 5.79. Found: C, 48.21; H, 5.72; N, 5.82. IR (KBr): 1655 (vs), 1610 (s), 1544 (s) 1462 (s), 1412 (vs), 1286 (s), 1234 (s), 1149 (m), 1103 (m), 1047 (w), 881 (m), 825 (m), 760 (w), 690 (m), 586 (m), 505 (w) $cm^{-1}$.

*$Mg_2$(dobpdc)(DEF)$_2$·DEF$_{1.5}$·$H_2O$ (DEF-2).* Into a 10-mL Pyrex cell, $H_4$dobpdc (24 mg, 0.088 mmol), $MgBr_2·6H_2O$ (60 mg, 0.21 mmol), and 3 mL of solvent (1:1 DEF:EtOH) were loaded and sealed with a PTFE cap. The mixture was irradiated in a microwave reactor (CEM Discover) for 30 min at 120 °C. After 30 min, the solution was cooled, and the resulting solid was collected via filtration and washed with hot DEF. The solid was dried under vacuum to yield 57.5 mg (95%) of product as a white powder. Anal. Calcd for $C_{31.5}H_{46.5}Mg_2N_{3.5}O_{10.5}$: C, 54.77; H, 6.78; N, 7.10. Found: C, 54.85; H, 7.07; N, 6.86. IR (KBr): 1661 (vs), 1612 (s), 1570 (s), 1468 (vs), 1419 (s), 1298 (s), 1242 (s), 1149 (m), 1111 (m), 1047 (w), 945 (w), 885 (m), 842 (m), 825 (m), 725 (w), 692 (m), 660 (w), 590 (m), 501 (w), 447 (w) $cm^{-1}$. Heating at 420 °C for 65 min *in vacuo* yielded the fully activated adsorbent $Mg_2$(dobpdc) (**2**).

*$Mg_2$(dobpdc)(mmen)$_{1.6}$($H_2O$)$_{0.4}$ (mmen-$Mg_2$(dobpdc) or mmen-2).* A sample of fully activated **2** (77 mg, 0.24 mmol) was immersed in anhydrous hexane, and 20 equiv of *N*,*N*′-dimethylethylenediamine (mmen, 0.53 mL, 4.8 mmol) was added. The suspension was stirred for one day, filtered, and rinsed copiously with hexanes. The solid was then evacuated of residual solvents at 100 °C for 24 h to afford 87 mg (77%) of product as a gray-white powder. Anal. Calcd for $C_{20.4}H_{26}Mg_2N_{3.2}O_{9.6}$: C, 52.46; H, 5.62; N, 9.60. Found: C, 52.15, H, 5.41; N, 9.52. IR (ATR, neat): 3320 (w), 2952 (w), 2910 (w), 2862 (w), 2806 (w), 1616 (s), 1575 (s), 1538 (w), 1468 (vs), 1421 (vs), 1295 (m), 1244 (s), 1152 (m), 1104 (m), 1053 (m), 1000 (w), 887 (m), 844 (m), 828 (m), 727 (w), 692 (s), 618 (m), 589 (s) $cm^{-1}$.

**X-ray Structure Determination.** A crystal of DEF-**1** was mounted on a cryoloop under a cooling stream of dinitrogen. Diffraction data were collected with synchrotron radiation using a 6B MX-I ADSC Quantum-210 detector with a silicon (111) double-crystal monochromator at the Pohang Accelerator Laboratory. The ADSC Quantum-210 ADX program (Ver. 1.92) was used for data collection and HKL2000 (Ver. 0.98.699) was used for cell refinement, data reduction, and absorption corrections. The structure was solved by direct methods and refined by full-matrix least-squares analysis using anisotropic thermal parameters for non-hydrogen atoms with the SHELXTL program.[33] The C2 and C5 atoms were isotropically refined due to poor thermal behavior. Guest molecules in the pores were highly disordered and unable to be modeled. To account for this electron density, the program SQUEEZE[34] was employed. All hydrogen atoms were calculated at idealized positions and refined using a riding model. Crystal data for DEF-**1**: empirical formula = $C_{12}H_{14}NO_4Zn$, $M_r$ = 301.61, $T$ = 100(2) K, space group = $P3_221$, $a$ = 21.698(3) Å, $c$ = 6.8690(14) Å, $\alpha$ = 90°, $\beta$ = 90°, $\gamma$ = 120°, $V$ = 2800.7(8) Å$^3$, $Z$ = 6, $D_{calc}$ = 1.073 g/cm$^3$, $\mu$ = 1.319 mm$^{-1}$, 13927 reflections collected, 2941 unique ($R_{int}$ = 0.0418), $R1$ = 0.0466, $wR2$ = 0.1204 ($I > 2\sigma(I)$).

**Powder X-ray Diffraction.** Powder X-ray diffraction data were collected with either a Rigaku Ultima III or a Bruker D8 Advance diffractometer using Cu K$\alpha$ radiation ($\lambda$ = 1.5406 Å). The unit cell dimensions of DEF-**2** and mmen-**2** were determined by performing a full-pattern decomposition using the Le Bail method, as implemented in TOPAS-Academic.[35] Owing to the isomorphism with $Zn_2$(dobpdc), the trigonal space group $P3_221$ was used for the refinements. Crystal data for DEF-**2**: $a$ = 21.761(2) Å, $c$ = 6.9721(7) Å, $V$ = 2859.1(5) Å$^3$ ($R_{wp}$ = 0.093, $R_p$ = 0.067). Crystal data for mmen-**2**: $a$ = 21.500(2) Å, $c$ = 6.8275(9) Å, $V$ = 2733.2(6) Å$^3$ ($R_{wp}$ = 0.042, $R_p$ = 0.033).

**Gas Adsorption Measurements.** Gas adsorption data for pressures in the range 0−1.1 bar were obtained by volumetric methods using a Micromeritics ASAP2020 instrument. All gases were 99.998% purity or higher. Isotherms at 77 K were measured in liquid nitrogen baths. Isotherms at 25, 35, 45, 50, and 75 °C were measured using liquid circulators to maintain a constant temperature. Isotherms at 100 and 120 °C were measured using a heated sand bath controlled by a programmable temperature controller. BET surface areas were calculated from $N_2$ adsorption at 77 K. DFT pore size distributions and pore sizes were calculated from $N_2$ adsorption at 77 K with the Micromeritics DFT Plus Models Kit (Ver. 2.02) software suite with cylinder pore geometries for an oxide surface. The compound mmen-**2** was regenerated at 100 °C under dynamic vacuum for 4 h after measurement of each isotherm.

**Isosteric Heats of Adsorption Calculations.** A dual-site Langmuir−Freundlich equation (eq 1) was employed to model the $CO_2$ adsorption at 25, 50, and 75 °C for mmen-**2** in the region before the step in the isotherms.

$$q = \frac{q_{sat,A} b_A p^{\alpha_A}}{1 + b_A p^{\alpha_A}} + \frac{q_{sat,B} b_B p^{\alpha_B}}{1 + b_B p^{\alpha_B}} \quad (1)$$

Here, $q$ is the amount of $CO_2$ adsorbed (mmol/g), $p$ is the pressure (bar), $q_{sat}$ is the saturation capacity (mmol/g), $b$ is the Langmuir−Freundlich parameter (bar$^{-\alpha}$), and $\alpha$ is the Langmuir−Freundlich exponent (dimensionless) for two adsorption sites A and B. In order to model the $CO_2$ adsorption in the region after the step, a modified Langmuir−Freundlich equation (eq 2) was employed.

$$q = \frac{q_{sat,A} b_A (p - p^*)^{\alpha_A}}{1 + b_A (p - p^*)^{\alpha_A}} + \frac{q_{sat,B} b_B (p - p^*)^{\alpha_B}}{1 + b_B (p - p^*)^{\alpha_B}} + \frac{q_{sat,C} b_C (p - p^*)^{\alpha_C}}{1 + b_C (p - p^*)^{\alpha_C}} \quad (2)$$

Here, adsorption is considered at three sites, A, B, and C, and the extra parameter $p^*$ is used to account for the pressure at which the step in the isotherm occurs and the strongest adsorption sites are first populated. After carefully refining the parameters in eqs 1 and 2, excellent agreement was achieved between the experimental isotherm data and the corresponding isotherm fits (see Figures S10−S13). Using the appropriate isotherm fits, Mathematica software was used to solve for the exact pressures, $p$, corresponding to constant amounts of $CO_2$ adsorbed, $q$, at 25, 50, and 75 °C. The Clausius−Clapeyron equation (eq 3) was then used to calculate the isosteric heats of adsorption, $Q_{st}$, by determining the slope of the best-fit line for ln $p$ versus $1/T$ at each loading.

$$(\ln p)_q = \left(\frac{Q_{st}}{R}\right)\left(\frac{1}{T}\right) + C \quad (3)$$

As indicated by the residual sum of square values, $R^2$, of close to 1 (see Figure S14), the isotherm data were consistent with the Clausius−Clapeyron equation across the entire loading range considered, even with the changes in the location of the step in the isotherms.

The isosteric heats of adsorption for $CO_2$ in the unmodified $Mg_2$(dobpdc) were determined by fitting the adsorption isotherms at 25, 35, and 45 °C with a dual-site Langmuir−Freundlich equation (eq 1). Each temperature was fit independently, and the Clausius−Clapeyron equation was used to determine $Q_{st}$ as a function of loading.

All fit parameters for $Mg_2$(dobpdc) and mmen-$Mg_2$(dobpdc) are specified in Tables S2−S4.

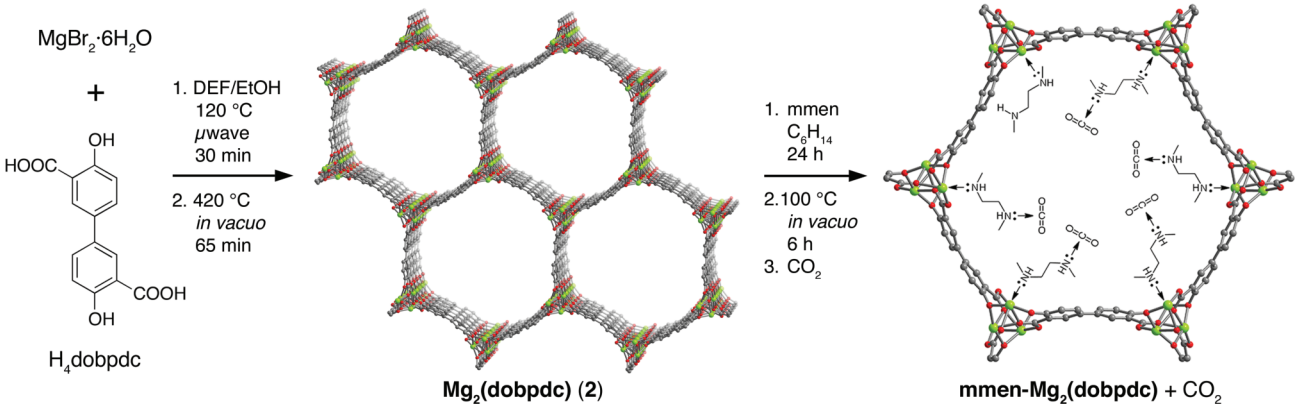


**Figure 1.** Synthesis of mmen-$Mg_2$(dobpdc) (mmen = *N,N′*-dimethylethylenediamine; $dobpdc^{4-}$ = 4,4′-dioxido-3,3′-biphenyldicarboxylate). From the microwave reaction of $MgBr_2 \cdot 6H_2O$ and $H_4$dobpdc (left), $Mg_2$(dobpdc) (**2**) is obtained following evacuation of the as-synthesized solid at high temperatures (middle). The framework structure depicted is that obtained from single crystal X-ray analysis of the isostructural zinc compound DEF-**1**. Green, red, and gray spheres represent Mg, O, and C atoms respectively; H atoms are omitted for clarity. Addition of an excess of mmen to the evacuated framework yields the amine-appended $CO_2$ adsorbent $Mg_2(dobpdc)(mmen)_{1.6}(H_2O)_{0.4}$ (right).

**Model $CO_2$ Isotherms.** Isotherms for $CO_2$ uptake in mmen-**2** at other temperatures were predicted from the experimental isotherm at 75 °C via application of a Clausius−Clapeyron relation (eq 4).

$$(\ln p_2) = \left( \frac{Q_{st} + \left( \ln p_1 \left( \frac{RT_1T_2}{T_2 - T_1} \right) \right)}{\left( \frac{RT_1T_2}{T_2 - T_1} \right)} \right) \quad (4)$$

Calculated pressures ($p_2$) at constant loadings ($q$) were determined assuming an isosteric heat of adsorption ($Q_{st}$) of 71 kJ/mol for all loadings. Here, $p_1$ is a pressure experimentally measured at 75 °C, $R$ is the universal gas constant, $T_1$ is 75 °C, and $T_2$ is the temperature for which a model isotherm is desired.

**$CO_2$ Selectivity Calculations.** Here, the adsorption capacities of component $n$ ($q_n$) are defined to be molar excess adsorption capacities determined experimentally without correction for absolute adsorption, and $p_n$ is defined to be the pressure of component $n$ as experimentally measured. Selectivity ($S$) is defined according to eq 5, while purity is defined according to eq 6.

$$S = \frac{q_{CO_2}/q_2}{p_{CO_2}/p_2} \quad (5)$$

$$\text{purity} = \frac{q_{CO_2}}{q_{CO_2} + q_2} \times 100\% \quad (6)$$

**Thermogravimetric Analysis and Gas Cycling Measurements.** Thermogravimetric analyses (TGA) were carried out at ramp rates between 5 and 10 °C/min under a nitrogen flow with a TA Instruments TGA Q5000 (Ver. 3.1 Build 246) or a Scinco TGA N-1000.

Carbon dioxide cycling experiments were performed on the aforementioned TA Instruments analyzer using 15% $CO_2$ in $N_2$ (Praxair NI-CD15C-K), 390 ppm $CO_2$ in air (Praxair AI-CD-390C-K; 390 ppm $CO_2$, 21% $O_2$, balance $N_2$), $CO_2$ (Praxair 99.998%), and $N_2$ (Praxair, 99.9%). A flow rate of 25 mL/min was employed for all gases. Prior to cycling, the sample was activated by heating at 150 °C for 1 h. For Figure 6, sample mass was normalized to be 0% at the adsorption temperature (25 °C for 390 ppm $CO_2$; 40 °C for 15% $CO_2$) under flowing $N_2$. For Figure 7, sample mass was normalized to be 0% at 150 °C under flowing 100% $CO_2$. Masses were uncorrected for buoyancy effects. In Figure 6, the difference between the quantity of $N_2$ adsorbed at the tare temperature and the regeneration temperature likely accounts for the negative apparent mass of mmen-**2** at high temperatures.

**Differential Scanning Calorimetry.** Thermal analysis was performed on a TA Instruments Q200 differential scanning calorimeter equipped with a refrigerated cooling system (RCS40). Through the sample cell, 15% $CO_2$ in $N_2$ or $N_2$ was flowed over T-Zero aluminum pans that were not hermetically sealed. An empty, aluminum T-Zero pan provided the reference sample for thermal analysis. The calorimeter was calibrated with the TA Instruments software package; the melting point of indium (156.60 °C) was utilized for the temperature calibration. Sample and pan masses were determined after activation at 150 °C for 60 min on a TA Instruments TGA Q5000 via the readout from the internal balance under flowing $N_2$. Identical aliquots of mmen-**2** were utilized for TGA and DSC measurements to approximate heats of adsorption. Integrated heats were calculated with TA Instruments Universal Analysis software suite.

**Other Physical Measurements.** Elemental analyses for C, H, and N were performed at the Elemental Analysis Service Center of Sogang University or the Microanalytical Laboratory of the University of California, Berkeley. $^1$H spectra were obtained using a 300 MHz Varian instrument. Infrared spectra were obtained from KBr pellets with a Bomen MB-104 spectrometer or on a Perkin-Elmer Spectrum 400 FTIR spectrometer equipped with an attenuated total reflectance (ATR) accessory. For diffuse reflectance infrared Fourier transform spectroscopy (DRIFTS) spectra, the Perkin-Elmer spectrometer was equipped a Harrick Praying Mantis Diffuse Reflectance accessory and a temperature-controlled high-pressure gas cell with Swagelok valves connecting 5% $CO_2$ in He (Praxair certified standard HE CD5C-K) and an oil-free vacuum.

## 3. RESULTS AND DISCUSSION

**Synthesis, Structure, and Activation.** Reaction of $H_4$dobpdc with $ZnBr_2 \cdot 2H_2O$ or $MgBr_2 \cdot 6H_2O$ in 1:1 DEF:EtOH afforded DEF-**1** and DEF-**2**, respectively (see Figure 1). The coordination environment of the divalent metal cations within **1** and **2** are analogous to those in the $M_2$(dobdc) series.[29] In the crystal structure of DEF-**1**, four different $dobpdc^{4-}$ ligands and one DEF molecule are bonded to each $Zn^{2+}$ ion in a distorted octahedral geometry. There are three unique O donor types from the $dobpdc^{4-}$ ligand: bridging ($\mu_2$) aryloxide O atoms (O1), bridging ($\mu_2$) carboxylate O atoms (O2), and nonbridging carboxylate O atoms (O3). The equatorial plane of each $Zn^{2+}$ is composed of two *trans*-disposed O1 ligands from different linkers, one O3 donor atom, and one O2 donor atom. An O2 donor atom occupies one axial coordination site, while the other axial site is occupied by an O donor atom from DEF, the reaction solvent. This coordination


dx.doi.org/10.1021/ja300034j | *J. Am. Chem. Soc.* 2012, 134, 7056−7065

mode results in the formation of helical chains of $Zn^{2+}$ atoms running along the *c* axis of the crystal. The resulting framework consists of a honeycomb lattice of hexagonal, one-dimensional channels approximately 18.4 Å in width. Bound DEF molecules occupy the $Zn^{2+}$ coordination sites along the corners of hexagonal channel walls. As shown in Figure S1, powder X-ray diffraction (PXRD) data indicate DEF-**2** to be isostructural with DEF-**1**.

Heating DEF-**2** at 420 °C for 65 min under dynamic vacuum, removed the DEF molecules bound to the metal atoms, completely activating the material and generating open $Mg^{2+}$ coordination sites. Such extreme thermal treatment was necessary because soaking in methanol at 100 °C for 20 h did not lead to exchange of the bound DEF molecules. The porosity of activated **2** was confirmed via $N_2$ adsorption at 77 K (see Figure S4), resulting in a BET surface area of 3270 $m^2/g$. Note that, in line with the expanded structure, this is significantly greater than the BET surface area of 1495 $m^2/g$ reported for $Mg_2$(dobdc).[36]

The synthesis and structure of mmen-**2** is depicted schematically at the right of Figure 1. An activated sample of **2** was suspended in hexanes and an excess of mmen was added. As shown by powder X-ray diffraction (see Figure S3), framework crystallinity was not significantly affected by activation or subsequent amine functionalization. A much reduced BET surface area of 70 $m^2/g$ was calculated for mmen-**2**, while DFT pore size distributions indicated a reduction in average pore size (see Figures S5–S7).

Upon exposure of DEF-**2** to atmospheric air, the white powder turns blue and a loss of crystallinity occurs, as observed via powder X-ray diffraction measurements. Amine functionalization, however, appears to enhance framework stability, because no similar degradation was observed for mmen-**2** upon exposure to air for one week.

**$CO_2$ Adsorption Isotherms.** The $CO_2$ adsorption data obtained for **2** are depicted in Figure S8. Isosteric heats of adsorption were calculated to approach −44 kJ/mol at low coverage, as shown in Figure S9. This value is similar to those previously reported for the analogous $Mg_2$(dobdc) framework.[37] The adsorption capacity of **2** at 25 °C is 4.85 mmol/g (17.6 wt %) and 6.42 mmol/g (22.0 wt %) at 0.15 and 1 bar, respectively. The gravimetric capacity of **2** for $CO_2$ at 0.15 bar exceeds the capacity of all metal–organic frameworks except for $Mg_2$(dobdc),[10c] which adsorbs 6.1 mmol/g (21.2 wt %) at 25 °C and 0.15 bar.[36]

The alkylamine-functionalized metal–organic framework mmen-**2** displayed an extremely high affinity for $CO_2$ at extraordinarily low pressures. The $CO_2$ adsorption isotherms obtained at 25, 50, and 75 °C are presented in Figure 2. At 25 °C and 0.39 mbar, near the current partial pressure of $CO_2$ in Earth's atmosphere, the compound adsorbed 2.0 mmol/g (8.1 wt %), which is 15 times the capacity of **2**. At the much higher pressure of 5 mbar, the median partial pressure of $CO_2$ within the International Space Station, the framework adsorbed 2.6 mmol/g (10.3 wt %). For comparison, zeolite 5A, which is currently used aboard the station to adsorb $CO_2$, adsorbs 0.85 mmol/g (3.6 wt %, crystallographic volumetric capacity 1.3 $mmol/cm^3$) at 5 mbar.[12,38]

At 25 °C, the $CO_2$ adsorption in mmen-**2** reaches 3.13 mmol/g (12.1 wt %) at 0.15 bar and 3.86 mmol/g (14.5 wt %) at 1 bar. Remarkably, its $CO_2$ uptake at 1 bar and 25 °C exceeds the amount of $N_2$ adsorbed at 77 K. Thus, the low surface area measured at 77 K does not appear to accurately reflect the surface area accessible to $CO_2$, and the pore size distribution calculated from $N_2$ adsorption at cryogenic temperatures likely does not accurately represent the true pore size distribution within mmen-**2**. On a per mass basis, the amine-functionalized framework adsorbed less $CO_2$ than **2** at pressures higher than 20 mbar. The large density difference between the two frameworks is primarily responsible for the lower gravimetric capacity of mmen-**2**. Crystallographic densities of 0.58 and 0.86 $g/cm^3$ were calculated for **2** and mmen-**2**, respectively. At 0.15 bar, **2** and mmen-**2** adsorb 2.8 and 2.7 $mmol/cm^3$, respectively.

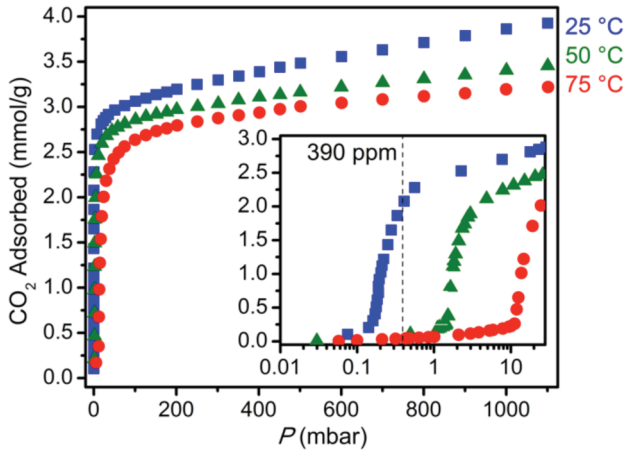


**Figure 2.** Adsorption of $CO_2$ in mmen-**2** at 25 °C (blue squares), 50 °C (green triangles), and 75 °C (red circles). Inset: The isotherms at very low pressures exhibit a step that shifts to higher pressures at higher temperatures. The dashed, vertical line marks the current partial pressure of $CO_2$ in air (390 ppm).

Based upon the calculated number of dangling amine groups in mmen-**2**, a loading of 3.4 mmol/g would correspond to one $CO_2$ per amine, yet uptake of only ca. 2.2 mmol/g was observed. Here, pore blockages, hydrogen bonded amines, or cooperative binding mechanisms between two amines and one $CO_2$ may be limiting the accessible stoichiometry of mmen-**2**. Thus, significant additional capacity improvements might be realized in the material if conditions can be identified for appending one mmen per magnesium and binding one $CO_2$ molecule per dangling amine.

Isosteric heat of adsorption calculations were hindered by the presence of a prominent step in the isotherms at low pressures and convex to the pressure axis. Generally, continuous mathematical functions are used to model experimental isotherms, which then become the input parameters for the Clausius–Clapeyron relation. Since we were unable to mathematically model the $CO_2$ isotherms of mmen-**2** with continuous equations over the entire pressure range, each isotherm was modeled with two Langmuir–Freundlich equations. Data sets corresponding to the adsorption regions before and after the steps were compiled and then modeled individually.

As shown in Figure 3, isosteric heats of adsorption for mmen-**2** were calculated from the 25, 50, and 75 °C isotherm models. At low loadings, heats significantly lower than those expected for chemical adsorption of $CO_2$ onto an amine were calculated. However, calculated heats quickly approached and maintained a value of −71 kJ/mol, which likely corresponds to the chemical adsorption of $CO_2$ onto the free amine of mmen. Here, a carbamate with a weak C–N bond is probably formed


dx.doi.org/10.1021/ja300034j | J. Am. Chem. Soc. 2012, 134, 7056–7065

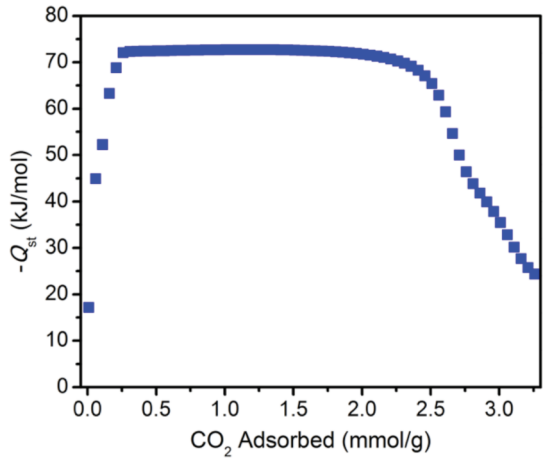


**Figure 3.** Isosteric heats of $CO_2$ adsorption onto mmen-**2**, as calculated using the Clausius–Clapeyron relation. The calculated values indicate that chemical adsorption of $CO_2$ onto the amines did not occur at very low coverage.

through interaction the lone pair of the free amine of mmen and the electrophilic carbon of $CO_2$.

*In situ* diffuse reflectance infrared Fourier transform spectroscopy (DRIFTS) was employed to probe the chemical nature of adsorbed $CO_2$. At 25 °C, 1 bar of 5% $CO_2$ in He was introduced into an airtight gas cell containing a sample of activated mmen-**2**. The difference spectrum between mmen-**2** under a 1 bar atmosphere and the activated framework under vacuum is shown in Figure 4. The prominent loss peak at 3316

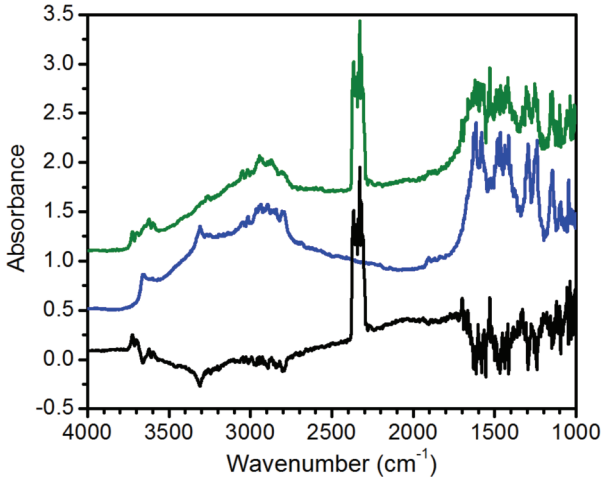


**Figure 4.** DRIFTS spectra of $CO_2$ adsorption in mmen-**2**. The loss band at 3316 $cm^{-1}$ in the difference spectrum (black line) between evacuated mmen-**2** (blue line) and mmen-**2** under a 5% $CO_2$ in He atmosphere (green line) indicates $CO_2$ adsorption occurs via a chemical adsorption mechanism. The blue line is offset by −0.5 absorbance units for visual clarity.

$cm^{-1}$, assigned to the NH stretch of free mmen-**2**, is indicative of chemical adsorption of $CO_2$ onto amines.

Recent work on alkylamine-grafted silica surfaces have suggested that chemical adsorption of $CO_2$ onto alkylamines is not possible without neighboring amines or surface hydroxyl groups to stabilize the resulting carbamates; ammonium carbamates or surface-bonded carbamates are formed, respectively.[39] The formation of surface-bonded carbamates in mmen-**2** is unlikely due to a lack of surface hydroxyl groups, and the broad NH stretches expected for ammonium cations are not definitively resolvable from the DRIFTS difference spectrum. Furthermore, the slow reversibility of mmen-**2** at room temperature (see Figure S15) appears to preclude the formation of ammonium carbamates, which have been reported to desorb $CO_2$ from primary amines readily at room temperature.[39] Additional experiments are necessary to ascertain whether adjacent functional groups are necessary for $CO_2$ adsorption within such alkylamine-functionalized metal–organic frameworks.

The step in each isotherm marks the pressure at which $CO_2$ adsorption becomes dominated by chemisorption. Interestingly, the step moves to significantly higher pressures as the adsorption temperature increases. As shown in Figure S16, the location of the step at 75 °C was reproduced four times with little variation. Thus, the step cannot be attributed to slow kinetics, but appears to be an inherent characteristic of mmen-**2** $CO_2$ adsorption isotherms. All batches of mmen-**2** have exhibited steps at approximately the same pressures, even when functionalized with different amounts of amines. Figure S17 presents the 75 °C $CO_2$ adsorption isotherm of $Mg_2(dobpdc)(mmen)_{1.75}(H_2O)_{0.25}$.

The location of the step is modeled well by a simple Clausius–Clapeyron relation (see eq 4), which predicts how isotherms move as a function of temperature. In Figure 5,

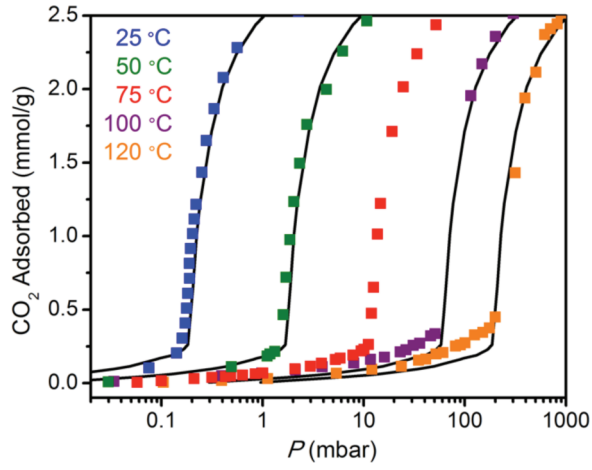


**Figure 5.** Adsorption of $CO_2$ in mmen-**2** at 25, 50, 75, 100, and 120 °C, represented as blue, green, red, purple, and orange squares, respectively. The locations of the step for the 25, 50, 100, and 120 °C isotherms were modeled with a Clausius–Clapeyron derived equation constructed from the 75 °C data (shown as black lines for each temperature). The heat of adsorption was assumed to be a constant −71 kJ/mol. The onset pressure of each isotherm step was predicted well by the simple model.

experimental isotherms at 25, 50, 75, 100, and 120 °C are shown as blue, green, red, purple, and orange squares, respectively. The black lines through the 25, 50, 100, and 120 °C data are predicted isotherms for those temperatures modeled from the experimental data collected at 75 °C by assuming that the heat of adsorption is −71 kJ/mol for all $CO_2$ loadings. The black lines are not continuous functions, but connect the calculated points listed in Table S5. Utilizing the approximate heat of adsorption calculated from the 25, 50, and 75 °C isotherms, the model was able to predict the general shapes of the 100 and 120 °C isotherms, as well as the


dx.doi.org/10.1021/ja300034j | *J. Am. Chem. Soc.* 2012, 134, 7056–7065

Table 1. Approximate $CO_2$ Selectivities of mmen-2 for Selected Gas Mixtures at 25 °C

| | | pressure (mbar) | | uptake (mmol/g) | | | |
|---|---|---|---|---|---|---|---|
| mixture | comp. 2 | $CO_2$ | comp. 2 | $CO_2$ | comp. 2 | molar selectivity | est. purity (%) |
| air | $N_2$ | 0.4 | 800 | 2.05 | 0.083 | 49 000 | 96 |
| air | $O_2$ | 0.4 | 200 | 2.05 | 0.038 | 27 000 | 98 |
| flue gas | $N_2$ | 150 | 750 | 3.13 | 0.079 | 200 | 98 |

pressures at which the steps arise. Thus, it seems that thermodynamics alone account for the movement of the step to higher pressures at higher temperatures.

The existence of the step, however, is unexpected in a strongly adsorbing material with large pores. The amines, as the strongest adsorption sites, should preferentially adsorb $CO_2$ before other, weaker adsorption sites adsorb significant quantities of $CO_2$. To explain the nonclassical adsorption behavior of mmen-**2**, we presently hypothesize that adsorption of $CO_2$ onto mmen is disfavored at low adsorptive concentrations (the density of gas phase $CO_2$ in the pores) because of the large positive entropy associated with reorganization of the amines, as required to form a chemical bond with $CO_2$. Before the chemical potential necessary for amine reorganization afforded to the system by the adsorptive is achieved, $CO_2$ adsorption is dominated by non-amine or weak amine-$CO_2$ adsorption sites. The minimum chemical potential required for amine reorganization increases as thermal motion increases, in line with the shift of the step to higher pressures at higher temperatures. Additional experiments and modeling will be required to test this hypothesis and to understand the relationship between pore filling and adsorption in mmen-**2**. However, the shift of the step to higher pressures at higher temperatures could afford the opportunity for unique regeneration conditions, whereby a weak vacuum could nearly fully regenerate the material at moderate temperatures.

**$CO_2$ Selectivity.** Adsorption isotherms for $N_2$ and $O_2$ in mmen-**2** at 25 °C are shown in Figure S18. The uptake capacities for these gases relative to $CO_2$ suggest that it would be a highly selective adsorbent. Since we were unable to mathematically model the $CO_2$ isotherms of mmen-**2** with a meaningful, single equation[40] over the entire pressure range of interest, ideal adsorbed solution theory (IAST)[41] selectivities could not be calculated. Table 1 therefore instead presents the approximate molar selectivities of mmen-**2** for relevant gas mixtures, as calculated according to eq 5 above using the excess adsorption capacities. This method for determining selectivities was recently shown to be less accurate than IAST, in part because it generally underestimates the values.[37]

The selectivity of mmen-**2** for $CO_2$ over $N_2$ in air is thus estimated to be at least 49 000. However, the purity of gas adsorbed is perhaps a more physically meaningful value than selectivity, and is an important criterion for evaluating adsorbents if captured $CO_2$ is to be transported or sequestered. The purity of $CO_2$ adsorbed onto mmen-**2**, calculated according to eq 6, would likely be more than 96% or 98% for capture from air or flue gas, respectively.

While the purity of gas adsorbed within individual mmen-**2** crystallites is very high, as shown in Table 1, the purity of gas adsorbed within a bed of adsorbent will be affected by the composition of gas phase molecules that fill the pore and intercrystalline spaces. For carbon capture applications, the high concentration of $N_2$ in these pore volumes will negatively affect the selectivity and purity values of real adsorbent beds. However, the approximate selectivity and purity values calculated in Table S6 indicate that the while the purity of $CO_2$ decreases within increasing void space, any adsorbent bed with less than 80% void space should be capable of achieving $CO_2$ purity in excess of 90%. From these calculations, we believe mmen-**2** to be a promising, high-capacity adsorbent for removing high-purity $CO_2$ from dry gas mixtures containing $N_2$ and $O_2$.

**$CO_2$ Capture from Air.** To evaluate the performance of mmen-**2** as a regenerable adsorbent, thermogravimetric analysis (TGA) was utilized to monitor sample mass under dynamic environments. The top panel of Figure 6 plots changes in sample mass (normalized to the mass of the framework under $N_2$ at 25 °C) while simulated air containing 390 ppm $CO_2$ was flowed over the sample. Despite the very low concentration of $CO_2$, a 4.6%$_{mc}$ (%$_{mc}$ = percent mass change;[42] 1.05 mmol/g; 4.4 wt %) was realized after 60 min. The adsorbent was then regenerated under flowing $N_2$ at 150 °C for 30 min and the cycle repeated 10 times with no apparent loss of capacity.

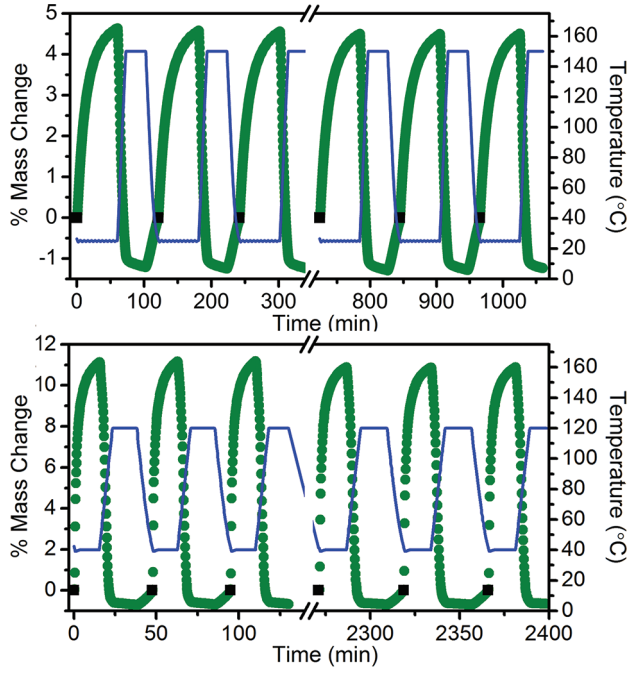


**Figure 6.** Adsorption–desorption cycling for mmen-**2**, demonstrating reversible uptake of 1.05 mmol $CO_2$/g from dry air after 1 h (upper) and 2.52 mmol $CO_2$/g from dry flue gas after 15 min (lower). Changes in sample mass are plotted as green circles and sample temperatures are plotted as blue lines; $CO_2$ was introduced into the sample chamber at the points marked by black squares. Samples were regenerated under flowing $N_2$.

To the best of our knowledge, no studies evaluating the efficacy of air capture within metal–organic frameworks have yet been reported. The equilibrium capacity (2.0 mmol/g, 1.72 mmol/cm$^3$) of mmen-**2** is similar to the capacities of the very best amine-grafted silica and alumina adsorbents reported to


dx.doi.org/10.1021/ja300034j | J. Am. Chem. Soc. 2012, 134, 7056–7065

date. However, the kinetics of adsorption appear to be significantly faster in mmen-**2** than for amines deposited via evaporation or polymerization methodologies. For example, while the pseudo-equilibrium capacity of an outstanding poly(ethyleneimine) impregnated silica gel was reported to be ca. 2.4 mmol/g, it took nearly 200 min for the silica based adsorbent to realize 4.6%$_{mc}$, the capacity of mmen-**2** for $CO_2$ after only 60 min.[23d] The easily accessed amines within mmen-**2** appear to enhance adsorption rates greatly, enabling rapid adsorption−desorption cycles to be utilized.

**$CO_2$ Capture from Dry Flue Gas.** The capabilities of mmen-**2** as an adsorbent for removing $CO_2$ from the flue gas of coal-fired power stations were also investigated. The bottom panel of Figure 6 presents the dynamic cycling behavior of mmen-**2** under the relevant, dry conditions: 15% $CO_2$ in $N_2$ flowing over the solid at 40 °C. After adsorbing $CO_2$ for 15 min, the sample was heated at 120 °C for 15 min under $N_2$. A capacity of 11.1%$_{mc}$ (2.52 mmol/g, 9.9 wt %) relative to the sample mass of mmen-**2** under $N_2$ at 40 °C was realized. After 50 cycles, only a 0.2%$_{mc}$ capacity loss was observed. Longer adsorption and desorption times did not significantly improve the cycling capacity of the material, nor did higher desorption temperatures. Note that the apparent capacity of mmen-**2** greatly exceeds the ca. 2 wt % working capacity[43] of aqueous monoethanolamine (MEA) scrubbers, which would likely swing between the same adsorption and desorption temperatures.

If captured $CO_2$ is to be sequestered, high-purity $CO_2$ is essential. To desorb the ca. 98% pure $CO_2$ adsorbed onto mmen-**2**, a $N_2$ or air purge cannot be utilized to strip the adsorbent bed. Hence, to approximate the working capacity of mmen-**2** using a temperature swing without a $N_2$ purge, a pure $CO_2$ purge was utilized instead. A 7.8%$_{mc}$ (1.8 mmol/g, 7.2 wt %) was realized when 15% $CO_2$ in $N_2$ at 40 °C was desorbed with 100% $CO_2$ at 150 °C. In Figure 7, 15% $CO_2$ was

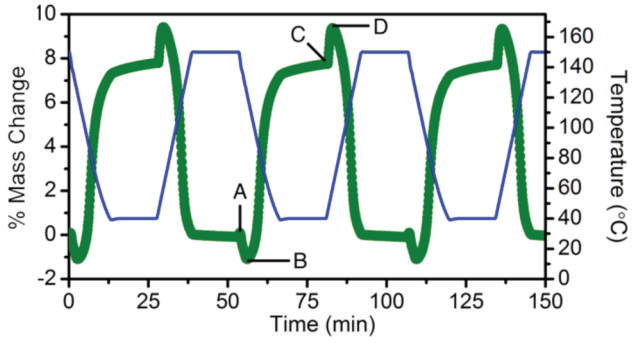


**Figure 7.** A temperature swing processes, as simulated for $CO_2$ in mmen-**2** using TGA and desorption with a $CO_2$ purge. A 1.8 mmol/g capacity difference was calculated from the quantity of $CO_2$ adsorbed at 150 °C under a 100% $CO_2$ atmosphere (point A) and the quantity of $CO_2$ adsorbed at 40 °C under flowing 15% $CO_2$ in $N_2$ (point C). Changes in sample mass are plotted as green circles and sample temperatures are plotted as blue lines; points B and D arise from introducing 15% $CO_2$ at 150 °C and 100% $CO_2$ at 40 °C respectively.

introduced over the sample at 150 °C (point A). The change in atmosphere from 100% to 15% $CO_2$ partially activated the framework, resulting in a negative effective mass (point B). As the sample cooled to 40 °C under the 15% atmosphere, $CO_2$ was adsorbed. After 15 min at 40 °C (point C), 100% $CO_2$ was introduced and the sample was heated at 10 °C/min. The increase in $CO_2$ concentration at low temperatures temporarily increased the amount of $CO_2$ adsorbed (point D). The working capacity of mmen-**2** is the difference between the amounts adsorbed at points A and C. The mass of the material at 150 °C under 100% $CO_2$ was normalized to be 0% mass in Figure 7. The relationship between points A and C and isotherms is illustrated in Figure S19.

**Differential Scanning Calorimetry.** To approximate the adsorbent regeneration energy, heats of adsorption and desorption were quantified for mmen-**2** via differential scanning calorimetry (see Figure 8).[44] When 15% $CO_2$ in $N_2$ at 40 °C

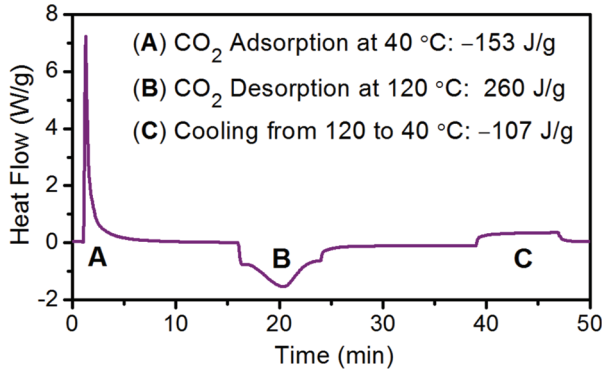


**Figure 8.** Heat flows from mmen-**2**, as determined via differential scanning calorimetry. First, 15% $CO_2$ in $N_2$ was adsorbed at 40 °C (event A). After 15 min, mmen-**2** was heated to 120 °C under $N_2$ (event B). Lastly, the regenerated material was cooled under $N_2$ to 40 °C (event C). The integrated heats calculated for each event are given in the legend.

was introduced over a sample of mmen-**2** activated at 150 °C under $N_2$, an exothermic heat flow of −153 J/g was observed (event A). Note that, to enable rapid gas exchange, the pan was not hermetically sealed and the true value of heats evolved are likely slightly larger than those registered by the instrument due to heat loss to the environment. When this heat flow was correlated to the 2.5 mmol/g capacity calculated via TGA adsorption under similar conditions, an approximate, average heat of adsorption of −61 kJ/mol $CO_2$ was calculated.

Following a 15 min adsorption period, 100% $N_2$ was introduced into the cell and the sample was heated to 120 °C (event B); 260 J/g were required to heat the sample and maintain the regeneration temperature for 15 min. Lastly, −107 J/g were evolved as the material was cooled under a $N_2$ atmosphere (event C) from 120 to 40 °C. Based upon this laboratory-scale experiment, approximately 2.34 MJ of energy would be required to regenerate 1 kg of $CO_2$ adsorbed onto mmen-**2**. This value compares very favorably with the 3.6−4.5 MJ of energy necessary to release 1 kg of $CO_2$ from an MEA scrubber.[5,43]

However, the aforementioned regeneration energies were measured under a $N_2$ purge, a laboratory-scale analogue for a temperature-vacuum swing regeneration cycle. While a direct measurement of regeneration energy with a 100% $CO_2$ purge was not possible, calculations shown in the SI indicate that the regeneration energy of mmen-**2** under $CO_2$ will be higher primarily due to the reduced working capacity of the adsorbent. The regeneration energy of mmen-**2** under $CO_2$ is still lower than the regeneration energy of the most highly optimized MEA solutions, and it is likely that optimization of adsorption and desorption temperatures will further lower the heat of regeneration of mmen-**2**.


dx.doi.org/10.1021/ja300034j | J. Am. Chem. Soc. 2012, 134, 7056−7065

Approximate heat capacities ($C_P$) were calculated for mmen-**2**. Over the 80 °C temperature range, the average heat required to regenerate $CO_2$-loaded mmen-**2** was 3.3 J/g·K. The regenerated framework released an average of 1.3 J/g·K upon cooling, a reasonable approximation of the heat capacity of mmen-**2**. For comparison, the heat capacity of a 30 wt % MEA solution without $CO_2$ is ∼3.8 J/g·K over the same 80 °C range.[43] The lower regeneration energy of mmen-**2** is thus attributable to its lower heat capacity. In addition, the significantly greater working capacity of mmen-**2** means that a smaller mass is required to adsorb the same amount of $CO_2$. The heat required to desorb $CO_2$ from the amines is similar for mmen-**2** and MEA solutions.[43]

## 4. CONCLUSIONS AND OUTLOOK

With the new metal−organic frameworks $M_2$(dobpdc) (M = Zn (**1**), Mg (**2**)), an expanded variant of the $M_2$(dobdc) (MOF-74) structure type has been achieved, leading to enlarged, 18.4-Å-wide channels lined with open metal coordination sites. Functionalization of **2** with mmen, afforded a remarkable new $CO_2$ adsorbent, mmen-$Mg_2$(dobpdc). The large capacity, high selectivity, and fast kinetics of this material for adsorbing $CO_2$ from dry gas mixtures with $N_2$ and $O_2$ make it an attractive new adsorbent for applications in which zeolites and inorganic bases are currently used, including the removal of $CO_2$ from air.

Future work will focus on evaluating the efficacy of alkylamine-appended metal−organic frameworks such as mmen-**2** under humid conditions. Whether the presence of water in gas mixtures will significantly affect the stability, capacity, selectivity, or regeneration energy of mmen-**2** is presently unknown. In addition, the peculiar $CO_2$ isotherm shapes warrant further investigation, since a detailed understanding of the adsorption behavior within mmen-**2** may enable the synthesis of even better materials for $CO_2$ capture. Finally, efforts are also underway to improve the separation performance of the material through use of various other polyamines in place of mmen.

## ■ ASSOCIATED CONTENT

### Supporting Information

Powder X-ray diffraction patterns and fits, additional $CO_2$, $N_2$, and $O_2$ isotherms and fits, FTIR spectra, TGA traces, and additional purity and regeneration energy calculations. This material is available free of charge via the Internet at http://pubs.acs.org.

## ■ AUTHOR INFORMATION

### Corresponding Author

cshong@korea.ac.kr; jrlong@berkeley.edu

### Notes

The authors declare no competing financial interest.

## ■ ACKNOWLEDGMENTS

The synthesis and characterization of compounds **1** and **2** was funded by the National Research Foundation of Korea (KRF-2009-220-C00021 and NRF20110018396) and PAL (2010-2063-04), while the remainder of this research, including the synthesis and characterization of mmen-**2**, was funded through the Center for Gas Separations Relevant to Clean Energy Technologies, an Energy Frontier Research Center funded by the U.S. Department of Energy, Office of Science, Office of Basic Energy Sciences, under Award No. DE-SC0001015. We also thank NSF for providing graduate fellowship support (J.A.M.). We thank Prof. T. Xu for use of the differential scanning calorimetry instrument.

## ■ REFERENCES

(1) National Oceanic and Atmospheric Administration. Trends in Atmospheric Carbon Dioxide. http://www.esrl.noaa.gov/gmd/ccgg/trends/ (accessed Nov 15, 2011).

(2) Carbon Dioxide Information Analysis Center. Recent Greenhouse Gas Concentrations. http://cdiac.ornl.gov/pns/ current_ghg.html (accessed Dec 16, 2011). DOI: 10.3334/CDIAC/atg.032.

(3) *Climate Change 2007: The Physical Science Basis*; Solomon, S., Qin, D., Manning, M., Chen, Z., Marquis, M., Averyt, K. B., Tignor, M., Miller, H. L., Eds.; The Fourth Assessment Report of the Intergovernmental Panel on Climate Change; Cambridge Univ. Press: New York, 2007.

(4) Chu, S. *Science* **2009**, *325*, 1599.

(5) *DOE/NETL Carbon Dioxide Capture and Storage RD&D Roadmap*; National Energy Technology Laboratory, 2010.

(6) Granite, E. J.; Pennline, H. W. *Ind. Eng. Chem. Res.* **2002**, *41*, 5470.

(7) Rochelle, G. T. *Science* **2009**, *325*, 1642.

(8) Fout, T.; Murphy, J. T. *DOE/NETL's Carbon Capture R&D Program for Existing Coal-Fired Power Plants*; DOE/NETL 2009/1356; National Energy Technology Laboratory, 2009.

(9) *Carbon Dioxide Capture from Existing Coal Fired Power Stations*; Revision Nov 2007; DOE/NETL 401/110907; National Energy Technology Laboratory, 2007.

(10) (a) D'Alessandro, D. M.; Smit, B.; Long, J. R. *Angew. Chem., Int. Ed.* **2010**, *49*, 6058. (b) Wang, Q.; Luo, J.; Zhong, Z.; Borgna, A. *Energy Environ. Sci.* **2011**, *4*, 42. (c) Sumida, K.; Rogow, D. L.; Mason, J. A.; McDonald, T. M.; Bloch, E. D.; Herm, Z. R.; Bae, T.-H.; Long, J. R. *Chem. Rev.* **2012**, *112*, 724.

(11) (a) Acharya, D. R.; Jain, R. *Sep. Sci. Technol.* **1995**, *30*, 3489. (b) Rege, S. U.; Yang, R. T.; Buzanowski, M. A. *Chem. Eng. Sci.* **2000**, *55*, 4827. (c) Kumar, R.; Huggahalli, M.; Deng, S.; Andrecovich, M. *Adsorption* **2003**, *9*, 243. (c) Kerry, F. G. *Industrial Gas Handbook: Gas Separation and Purification*. CRC: Boca Raton, 2007.

(12) International Zeolite Association. *Database of Zeolite Structures*. http://www.iza-structure.org/databases/ (Accessed Dec 30, 2011).

(13) (a) Carhart, H. W.; Thompson, J. K. *Removal of Trace Contaminants from Air*; ACS Symposium Series *17*; American Chemical Society: Washington, DC, 1975; p 1. (b) Wieland, P. O. Controlling Carbon Dioxide. *Living Together in Space: The Design and Operation of the Life Support Systems on the International Space Station*; NASA/TM-98-206956/VOL1; NASA Marshall Space Flight Center: Marshall Space Flight Center, AL, 1998; Chapter 3.3.1, p 121.

(14) Law, J.; Watkins, S.; Alexander, D. *In Flight Carbon Dioxide Exposures and Related Symptoms: Association, Susceptibility, and Operational Implications*; NASA/TP-2010-216126; NASA: Hanover, MD, 2010.

(15) Carbon Dioxide. *NIOSH Pocket Guide to Chemical Hazards*; NIOSH Publication 2005-149; Department of Health and Human Services, Centers for Disease Control and Prevention, National Institute for Occupational Safety and Health: Cincinnati, OH, 2007.

(16) Ahuja, V.; Green, R. *Int. J. Hydrogen Energy* **1998**, *23*, 131.

(17) Goeppert, A.; Czaun, M.; May, R. B.; Prakash, G. K. S.; Olah, G. A.; Narayanan, S. R. *J. Am. Chem. Soc.* **2011**, *133*, 20164.

(18) McLean, G. F.; Niet, T.; Prince-Richard, S.; Djilali, N. *Int. J. Hydrogen Energy* **2002**, *27*, 507.

(19) Keith, D. *Science* **2009**, *325*, 1654.

(20) (a) Jones, C. W. *Annu. Rev. Chem. Biomol. Eng.* **2011**, *2*, 31. (b) Ranjan, M.; Herzog, H. J. *Energy Procedia* **2011**, *4*, 2869.

(21) American Physical Society. *Direct Air Capture of $CO_2$ with Chemicals*. http://www.aps.org/policy/reports/assessments/upload/dac2011.pdf (accessed Nov. 20, 2011).

(22) (a) Satyapal, S.; Filburn, T.; Trela, J.; Strange, J. *Energy Fuels* **2001**, *15*, 250. (b) Schaldt, M. J.; Filburn, T. P.; Helble, J. J. *Ind. Eng. Chem. Res.* **2007**, *46*, 1590.
(23) (a) Belmabkhout, Y.; Serna-Guerrero, R.; Sayari, A. *Chem. Eng. Sci.* **2010**, *65*, 3695. (b) Choi, S.; Drese, J. H.; Eisenberger, P. M.; Jones, C. W. *Environ. Sci. Technol.* **2011**, *45*, 2420. (c) Chaikittisilp, W.; Lunn, J. D.; Shantz, D. F.; Jones, C. W. *Chem.—Eur. J.* **2011**, *17*, 10556. (d) Choi, S.; Gray, M. L.; Jones, C. W. *ChemSusChem* **2011**, *4*, 628. (e) Stuckert, N. R.; Yang, R. T. *Environ. Sci. Technol.* **2011**, *45*, 10257. (f) Wurzbacker, J. A.; Gebald, C.; Steinfeld, A. *Energy Environ. Sci.* **2011**, *4*, 3584.
(24) Chaikittisilp, W.; Kim, H.-J.; Jones, C. W. *Energy Fuels* **2011**, *25*, 5528.
(25) Gebald, C.; Wurzbacher, J. A.; Tingaut, P.; Zimmermann, T.; Steinfeld, A. *Environ. Sci. Technol.* **2011**, *45*, 9101.
(26) Wang, T.; Lackner, K. S.; Wright, A. *Environ. Sci. Technol.* **2011**, *45*, 6670.
(27) (a) Li, J.-R.; Kuppler, R. J.; Zhou, H.-C. *Chem. Soc. Rev.* **2009**, *38*, 1477. (b) Keskin, S.; van Heest, T. M.; Sholl, D. S. *ChemSusChem* **2010**, *3*, 879.
(28) (a) Chen, B.; Ockwig, N. W.; Millward, A. R.; Contreras, D. S.; Yaghi, O. M. *Angew. Chem., Int. Ed.* **2005**, *44*, 4745. (b) Dincă, M.; Dailly, A.; Liu, Y.; Brown, C. M.; Neumann, D. A.; Long, J. R. *J. Am. Chem. Soc.* **2006**, *128*, 16876. (c) Bae, Y.-S.; Farha, O. K.; Spokoyny, A. M.; Mirkin, C. A.; Hupp, J. T.; Snurr, R. Q. *Chem. Commun.* **2008**, 4135. (d) Llewellyn, P. L.; Bourrelly, S.; Serre, C.; Vimont, A; Daturi, M; Hamon, L; Weireld, G. D.; Chang, J.-S.; Hong, D.-Y.; Hwang, Y. K.; Jhung, S. H.; Férey, G. *Langmuir* **2008**, *24*, 7245. (e) Yazaydin, A. Ö.; Benin, A. I.; Faheem, S. A.; Jakubczak, P.; Low, J. J.; Willis, R. R.; Snurr, R. Q. *Chem. Mater.* **2009**, *21*, 1425.
(29) (a) Rosi, N. L.; Kim, J.; Eddaoudi, M.; Chen, B. L.; O'Keeffe, M.; Yaghi, O. M. *J. Am. Chem. Soc.* **2005**, *127*, 1504. (b) Dietzel, P. D. C.; Morita, Y.; Blom, R.; Fjellvag, H. *Angew. Chem., Int. Ed.* **2005**, *44*, 6354. (c) Dietzel, P. D. C.; Panella, B.; Hirscher, M.; Blom, R.; Fjellvag, H. *Chem. Commun.* **2006**, 959. (d) Zhou, W.; Wu, H.; Yildrim, T. *J. Am. Chem. Soc.* **2008**, *130*, 15268. (e) Bloch, E. D.; Murray, L. M.; Queen, W. L.; Chavan, S.; Maximoff, S. N.; Bigi, J. P.; Krishna, R.; Peterson, V. K.; Grandjean, F.; Long, G. J.; Smit, B.; Bordiga, S.; Brown, C. M.; Long, J. R. *J. Am. Chem. Soc.* **2011**, *133*, 14814.
(30) (a) Hwang, Y. K; Hong, D.-Y.; Chang, J.-S.; Jhung, S. H.; Seo, Y.-K.; Kim, J.; Vimont, V.; Daturi, M.; Serre, C.; Férey, G. *Angew. Chem., Int. Ed.* **2008**, *47*, 4144. (b) Demessence, A.; D'Alessandro, D. M.; Foo, M. L.; Long, J. R. *J. Am. Chem. Soc.* **2009**, *131*, 8784. (c) Wiers, B. M.; Foo, M.-L.; Balsara, N. P.; Long, J. R. *J. Am. Chem. Soc.* **2011**, *133*, 14522.
(31) McDonald, T. M.; D'Alessandro, D. M.; Krishna, R.; Long, J. R. *Chem. Sci.* **2011**, *2*, 2022.
(32) Tomic, E. A. *J. Appl. Polym. Sci.* **1965**, *9*, 3745.
(33) Sheldrick, G. M. *SHELXTL*, Version 6.12; Bruker Analytical X-Ray Systems, Inc.: Madison, WI, 2000.
(34) Van der Sluis, P.; Spek, A. L. *Acta Crystallogr., Sect. A* **1990**, *46*, 194.
(35) Coelho, A. *TOPAS-Academic*, Version 4.1; Coelho Software: Brisbane, 2007.
(36) Caskey, S. R.; Wong-Foy, A. G.; Matzger, A. J. *J. Am. Chem. Soc.* **2008**, *130*, 10870.
(37) Mason, J. A.; Sumida, K.; Herm, Z. R.; Krishna, R.; Long, J. R. *Energy Environ. Sci.* **2011**, *4*, 3030.
(38) Mulloth, L. M; Finn, J. E. *Carbon Dioxide Adsorption on a 5A Zeolite Design for $CO_2$ Removal in Spacecraft Cabins*; NASA/TM-1998-208752; NASA Ames Research Center: Moffett Field, CA, 1998.
(39) Danon, A.; Stair, P. C.; Weitz, E. *J. Phys. Chem. C* **2011**, *115*, 11540.
(40) While virial-type equations were capable of describing the $CO_2$ isotherm data for mmen-**2** at each temperature independently, unsuitably large numbers of parameters were required for good fits to be obtained.
(41) Myers, A. L.; Prausnitz, J. M. *AIChE J.* **1965**, *11*, 121.
(42) In this work, weight percent (wt %) is defined as

$$\text{wt\%} = \frac{\text{mass of adsorbate}}{\text{mass of adsorbate} + \text{mass of adsorbent}} \times 100\% \quad (8)$$

The mass change registered by the TGA does not account for adsorbate mass in the denominator and thus is not strictly wt %. To clearly differentiate this difference, the abbreviation $\%_{mc}$ (percent mass change) is used instead to describe the experimentally observed mass changes. As an additional note, because TGA only records net mass change, the mass of $N_2$ in the activated framework likely displaced by $CO_2$ is not registered as part of the $\%_{mc}$.
(43) Song, H.-J.; Lee, S.; Park, K.; Lee, J.; Spah, D. C.; Park, J.-W.; Filburn, T. P. *Ind. Eng. Chem. Res.* **2008**, *47*, 9925.
(44) Mu, B.; Walton, K. S. *J. Phys. Chem. C* **2011**, *115*, 22748.